Publication IV

K. Uusi-Esko, M. Karppinen, Extensive Series of Hexagonal and Orthorhombic *R*MnO_3 (*R* = Y, La, Sm, Tb, Yb, Lu) Thin Films by Atomic Layer Deposition, Chem. Mater. 23 (2011) 1835-1840.

CHEMISTRY OF MATERIALS

ARTICLE

pubs.acs.org/cm

Extensive Series of Hexagonal and Orthorhombic $RMnO_3$ (R = Y, La, Sm, Tb, Yb, Lu) Thin Films by Atomic Layer Deposition

Kristina Uusi-Esko and Maarit Karppinen*

Laboratory of Inorganic Chemistry, Department of Chemistry, Aalto University, P.O. Box 16100, FI-00076 Aalto, Finland

ABSTRACT: Atomic layer deposition (ALD) with subsequent annealing in N_2 gas flow was employed to fabricate an extensive series of both hexagonal and orthorhombic rare-earth manganate $RMnO_3$ thin films using $R(thd)_3$, $Mn(thd)_3$, and ozone as precursors. Excellent control of the R/Mn stoichiometry was achieved for all the rare-earth constituents studied at 275 °C. The formation of the metastable perovskites was elegantly enhanced through depositions on coherent perovskite substrates resulting in a complete series (from R = La to Lu) of single-phase $RMnO_3$ perovskites on $LaAlO_3$ substrates. The magnetic properties of the perovskite series exhibited expected antiferromagnetic behaviour at low temperatures (except for R = La which showed ferromagnetic interactions due to cation vacancies).

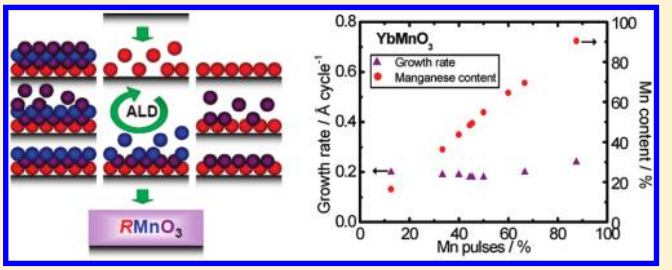

KEYWORDS: atomic layer deposition, thin films, ternary manganese oxides, crystal structure, magnetic property

1. INTRODUCTION

The rare-earth (R) manganese oxides are an interesting family of materials that can be structurally divided into two groups based on the size of the R constituent: for the larger rare earths (La−Dy), orthorhombic perovskite structure is adopted whereas the smaller rare earths (Sc, Y, Ho−Lu) crystallize in a hexagonal structure when prepared under ambient pressure.[1,2] The wide interest toward the hexagonal *h*-$RMnO_3$ series has largely been due to the coexistence of antiferromagnetic (AFM) ordering of the Mn^{III} moments and the ferroelectric polarization along the *c*-axis at low temperatures.[3−6] The fairly uncommon situation has its origin in the noncentrosymmetric structure involving the buckling observed in the R plane which is increased with decreasing size of the rare-earth element. The orthorhombic structure, on the other hand, compensates the decreasing size of the R constituent through the distortion of the oxygen sublattice leading to increasing tilts of the MnO_6 octahedra. The nondoped orthorhombic *o*-$RMnO_3$ phases are antiferromagnetic insulators; however, the preparation of stoichiometric samples can be challenging in the case of the largest members of the rare-earth series. Moreover, the stoichiometric samples are often not even desired as the exciting functional properties only emerge upon increasing the concentration of Mn^{IV} on the expense of Mn^{III}. As soon as cation vacancies are formed in the structure, the presence of Mn^{IV} gives rise to ferromagnetism (FM), improving also the electrical conductivity and colossal magnetoresistance.[7−9] In addition to colossal magnetoresistance, the orthorhombic $RMnO_3$ phases are known for their catalytic properties, e.g., as combustion catalysts.[10,11]

Atomic layer deposition (ALD) offers an excellent method for producing a coating that is not only uniform and conformal on large uneven surfaces but also is a technique that enables excellent control of the film thickness and stoichiometry.[12] The benefits of ALD are mainly derived from the self-limiting growth mechanism, which is achieved through alternate pulsing of the precursors. Thus, gas-phase reactions are eliminated, and the growth proceeds exclusively via surface reactions. The number of ternary oxide processes developed for ALD has been steadily increasing in recent years. Most of the work has been performed on the immensily versatile perovskite family of oxides. In the present work, a method has been developed for fabricating both hexagonal and orthorhombic $RMnO_3$ thin films through ALD and postdeposition heat treatment. To the author's knowledge, it is the first time such an extensive series of rare-earth manganites from lanthanum to lutetium has been prepared by any thin film fabrication method. In addition to an elegant way for producing metastable perovskites of o-$RMnO_3$ of the smaller rare earths, the magnetic properties of the o-$RMnO_3$ perovskite series have been studied.

Table 1. Deposition Temperatures (T_{dep}) and Precursor ($R(thd)_3$) Evaporation Temperatures (T_{sub}) Used in the Depositions of $R_xMn_yO_3$ Thin Films[a]

R	T_{sub}/°C	T_{dep}/°C	GPC/Å cycle^{-1}
La	162	275	0.23
Sm	139−141	275	0.23
Tb	128−130	250−325	0.18
Y	123	225−350	0.18
Yb	123	275−300	0.18
Lu	123	275−300	0.18

[a] The growth-per-cycle (GPC) values are for the $RMnO_3$ films deposited at 275 °C with a R/Mn pulsing ratio of 1:1.

Received: December 6, 2010
Revised: February 7, 2011
Published: March 02, 2011

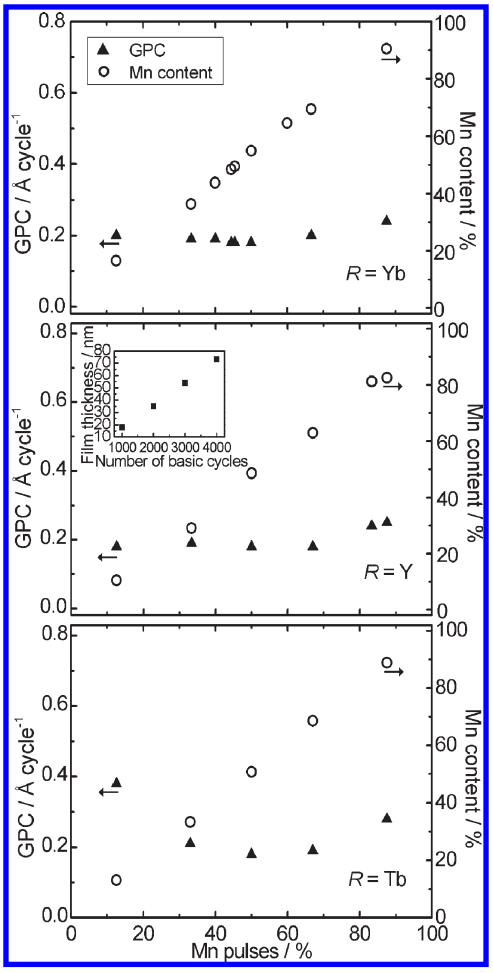

Figure 1. Effect of the precursor pulsing ratio on the actual Mn content (○) and the growth-per-cycle (GPC) value (▲) of $R_xMn_yO_3$ (R = Yb, Y, Tb) films at deposition temperature of 275 °C. The inset shows the dependence of the $Y_xMn_yO_3$ (with a Y/Mn pulsing ratio of 1:1) film thickness on the number of basic ALD cycles.

2. EXPERIMENTAL SECTION

Thin film depositions of $R_xMn_yO_3$ with R = Y, La, Sm, Tb, Yb, and Lu were performed using a commercial flow-type ALD reactor (F-120 by ASM Microchemistry Ltd.) under a pressure of 2−3 mbar. In order to study the ALD process of rare-earth manganites, the deposition temperature was varied between 225 and 350 °C (Table 1). Most of the depositions were, however, carried out at 275 °C to allow reasonable comparison of the film properties. On the basis of earlier studies for R = La[13,14] and Y[15] and preliminary depositions performed for the present work, self-limiting ALD-type growth was found to take place at the chosen deposition temperature of 275 °C. The metal precursors used in this study were $R(thd)_3$ and $Mn(thd)_3$ synthesized according to methods described in refs 16 and 17 and purified by sublimation. The alternating precursor pulses of metal and oxygen sources were introduced into the reactor using nitrogen as a carrier and purging gas. Ozone, used as an oxygen source, was generated from oxygen (>99.999%) in an ozone generator (Fischer model 502). The concentration of ozone was ca. 10% (60 g/m^3), and the gas flow rate during the pulse was about 60 cm^3/min as measured for the oxygen gas. Nitrogen (>99.999%) gas was generated in a Schmidlin UHPN 3000 N_2 generator. The films were deposited on single-crystal substrates of $LaAlO_3$(100) (pseudocubic, a = 3.79 Å), $SrTiO_3$(100) (cubic, a = 3.91 Å), and Si(100). The precursor ($R(thd)_3$) evaporation temperatures (T_{sub}) and substrate temperatures

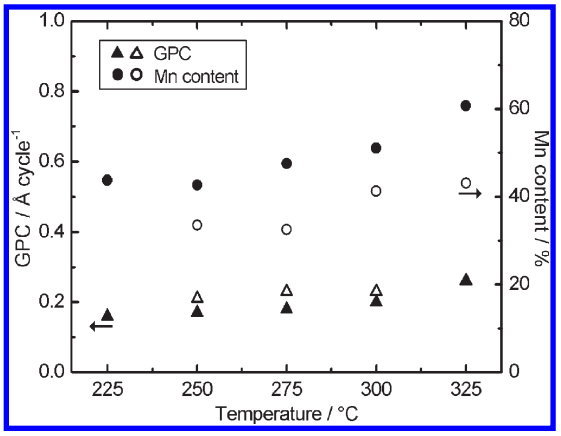

Figure 2. Temperature dependencies of the growth-per-cycle (GPC) value (triangles) and the Mn content (circles) for $R_xMn_yO_3$ (R = Y, Tb) deposited with a R/Mn pulsing ratio of 1:1 (the number of basic ALD cycles was 2000). Filled symbols refer to $Y_xMn_yO_3$ and open symbols to $Tb_xMn_yO_3$.

(T_{dep}) together with the growth-per-cycle (GPC) values for each of the materials are listed in Table 1. Process parameters, such as precursor pulsing and purging times, used in the depositions were partly adopted from earlier studies on ALD of $YMnO_3$, Y_2O_3, and MnO_x[15,18,19] and were generally found to apply well for the entire series of $RMnO_3$. A basic ALD cycle consisted of the following sequence: 1.5 s $R(thd)_3$ followed by 1.5 s purge or 2.0 s $Mn(thd)_3$ followed by 2.0 s purge, 1.5 s ozone, and 1.8 s purge. The film thickness after 1000 basic cycles was typically about 20 nm. The pulsing schemes were alternated to facilitate optimal mixing of the metal components. As most of the as-deposited films were amorphous, selected films were annealed after deposition in a rapid thermal annealing (RTA) furnace PEO 601 (ATV Technologie GmbH) in N_2 flow. The heat-treatment temperature varied between 600 and 1000 °C.

The actual Mn content against the total metal content, i.e., $y/(x+y)$, was measured by an X-ray fluorescence (XRF) spectrometer (Philips PW 1480 WDS) using Rh excitation. The data were analyzed with the UniQuant software which utilizes a DJ Kappa model to calculate simultaneously the composition and the mass thickness of an unknown bulk or thin-film sample.[20] The thicknesses of the $R_xMn_yO_3$ films were determined by X-ray reflectivity (XRR) using Panalytical X'Pert Pro MPD Alpha-1 powder diffractometer with Cu Kα1 radiation. The X-ray diffraction (XRD) measurements were performed with a Philips MPD 1880 powder diffractometer using Cu Kα radiation. The lattice parameters were obtained from profile fitting with the FULLPROF software.[21] Magnetization of the $R_xMn_yO_3$ thin-film samples was studied with a superconducting quantum interference device (SQUID) magnetometer by Quantum Design: MPMS-XL5. The samples for SQUID measurements were prepared by depositing 200 nm of $R_xMn_yO_3$ on the substrate material mounted on a plastic straw with film surface perpendicular to the direction of the applied field. The temperature dependence of magnetization was measured in both field-cooled (FC) and zero-field-cooled (ZFC) modes under a magnetic field of 1000 Oe.

3. RESULTS AND DISCUSSION

The fabrication of $R_xMn_yO_3$ thin films by ALD was successful for the entire series, and the films were of high-quality showing no significant gradients in either thickness or Mn content. The linear dependence of $Y_xMn_yO_3$ film thickness on the number of basic ALD cycles (deposited at 275 °C) is demonstrated in the inset of Figure 1. The constant GPC or growth-per-cycle value

Table 2. Effect of the Substrate Material on the Crystal Structure of $RMnO_3$ with R = Y, La, Sm, Tb, Yb, Lu (after Post-Deposition Annealing in N_2)

R	deposited on Si	deposited on $LaAlO_3$	deposited on $SrTiO_3$
La	*r*-$LaMnO_3$	*r*-$LaMnO_3$	
Sm	*o*-$SmMnO_3$	*o*-$SmMnO_3$	*o*-$SmMnO_3$
T	*o*-$TbMnO_3$	*o*-$TbMnO_3$	$Tb_2Mn_2O_7$ or $TbMn_2O_5$
Y	*h*-$YMnO_3$, Y_2O_3, MnO_2, Mn_2O_3	*o*-$YMnO_3$	*o*-$YMnO_3$
Yb	*h*-$YbMnO_3$	*o*-$YbMnO_3$	*o*-$YbMnO_3$, *h*-$YbMnO_3$
Lu	*h*-$LuMnO_3$	*o*-$LuMnO_3$	

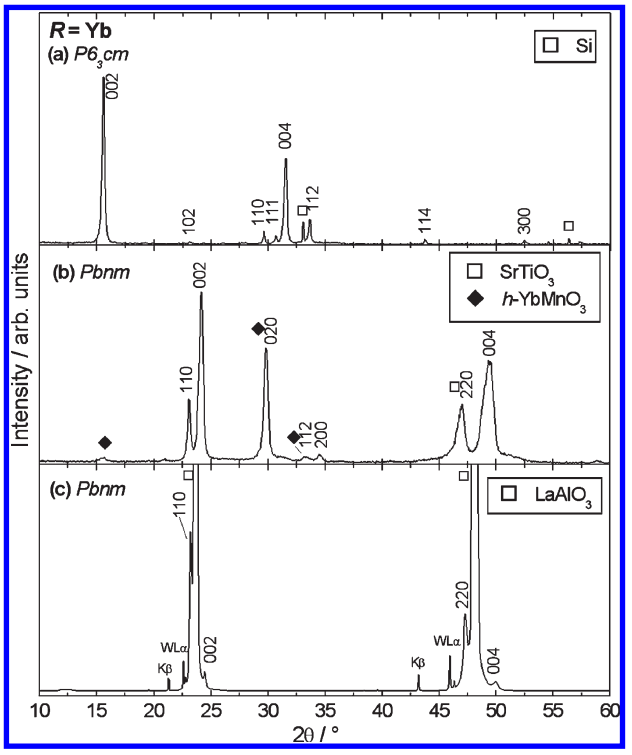

Figure 3. XRD patterns for annealed $YbMnO_3$ films deposited on (a) Si(100), (b) $SrTiO_3$(100), and (c) $LaAlO_3$(100) substrates. The indices are for the hexagonal space group $P6_3cm$ in (a) and for the orthorhombic space group *Pbnm* in (b) and (c). The film thickness was 200 nm.

confirms that the thickness of the films can be controlled simply by monitoring the number of deposition cycles. Depositions performed at 275 °C showed moreover excellent control of the cation stoichiometry as seen in Figure 1 for R = Yb, Y, and Tb. Although it is often found that the film composition has a slightly nonlinear dependency on the ALD precursor pulsing ratio, in the case of $R_xMn_yO_3$ (with R = Tb, Yb), this dependency is extremely close to linear. In contrast to our previous work on $YMnO_3$,[15] it was found that even highly Mn-rich films (with Mn content up to 88%) could be deposited in a well-controlled manner if the temperature was kept at 275 °C or below and the ozone pulsing was sufficient. In general, it is quite evident that the GPC value tends to increase with increasing Mn content for all the $R_xMn_yO_3$ systems deposited in this study, probably due to the rapidly increasing GPC of binary manganese oxide at temperatures above 240 °C.[22] In addition, the GPC is also increased while

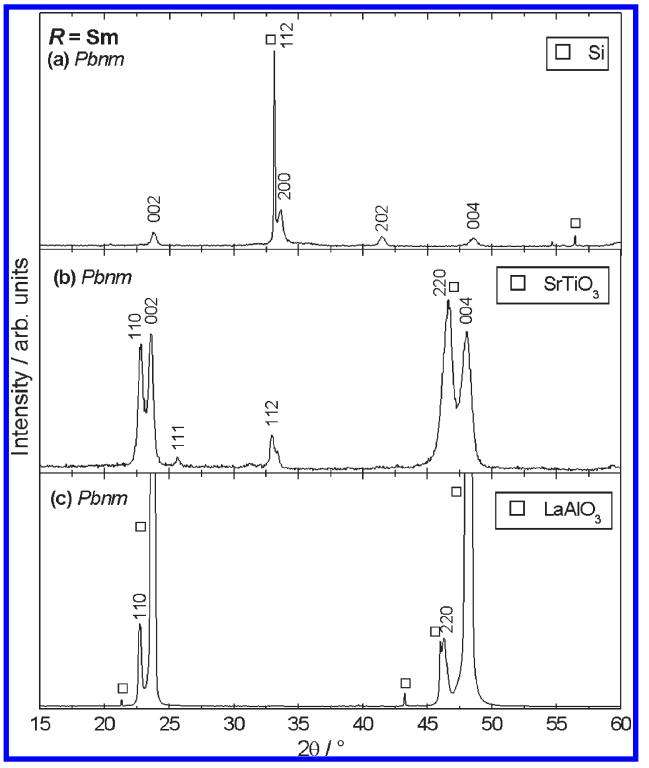

Figure 4. XRD patterns for annealed $SmMnO_3$ films deposited on (a) Si(100), (b) $SrTiO_3$(100), and (c) $LaAlO_3$(100) substrates. The indices are for the orthorhombic space group *Pbnm*. The film thickness was 200 nm.

depositing highly terbium-rich $Tb_xMn_yO_3$ films. X-ray diffraction analysis performed on as-deposited samples reveals the presence of terbium oxide in the films. Although the ALD processes are known for most of the binary rare-earth oxides, terbium oxide is an exception. A few TbO_x depositions were performed in this study and, as the films were visibly thinner toward the edges of the silicon substrate, it was evident that no well-controlled growth could be observed at the attempted temperature range of 250−325 °C. The GPC of terbium oxide at 275 °C was found to be ~0.6 Å/cycle, which would well explain our observation of increasing growth rate of $Tb_xMn_yO_3$ with increasing Tb content.

The GPC values for the entire series of rare-earth manganites are presented in Table 1. It is well-known that the GPCs of binary rare-earth oxides increase with increasing size of ionic radius $r(R^{III})$ from 0.21 Å/cycle for Tm up to 0.44 Å/cycle for Nd.[23,24] The GPC is increased not only because of the increasing size of the R constituent but also due to other factors including the tendency of larger rare earths to adopt higher coordination numbers leading to dimerization of their $R(thd)_3$ complexes.[25−27] In the case of the $RMnO_3$ series, the increase in GPC is somewhat less pronounced compared to binary rare-earth oxides but still greater than what can be explained simply by the increasing ionic radius $r(R^{III})$.

Our earlier studies on $YMnO_3$[15] have given some indication of the increase in Mn content with increasing temperature. As seen in Figure 2, the same is observed also for $TbMnO_3$ thin films and it is quite clear that the ALD processes of these ternary manganites are sensitive to changes in temperature. Fortunately, the changes in Mn content and GPC are not too significant, and moreover, it should be noted that the processes are reproducible at a specific temperature as long as the heating of the ALD reactor

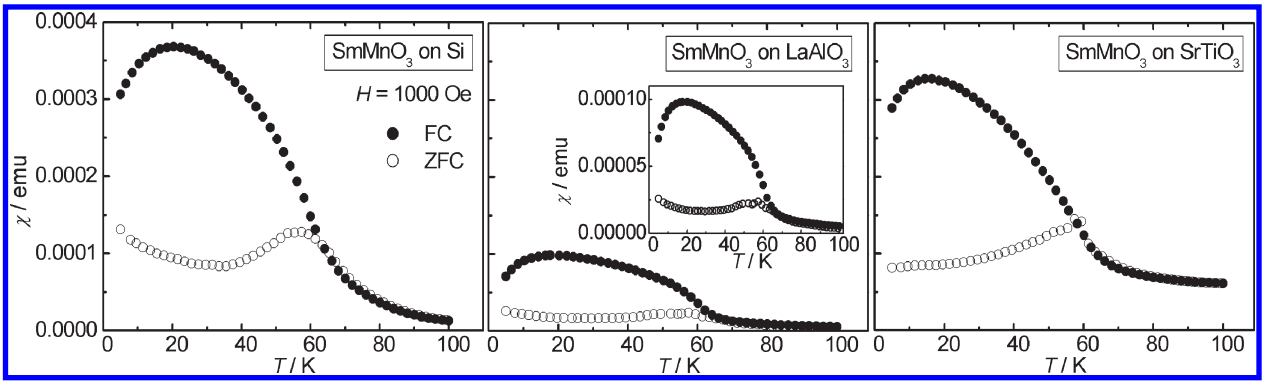

Figure 5. Temperature dependence of magnetic susceptibility (χ) in ZFC and FC modes under an external field of 1000 Oe for $SmMnO_3$ thin-film samples deposited on silicon, $LaAlO_3$, and $SrTiO_3$.

is reliable and reproducible. Any changes in reactor configuration tend to affect the cation ratio of the films; however, the dependency between the film composition and the ALD pulsing ratio (Figure 1) should not be affected. In the case of $RMnO_3$, the film composition should always have a close to linear dependency on the ALD pulsing ratio, thus, depositing a film with a specific composition should be rather an easy task to achieve. According to Figure 2, the temperature range of constant GPC of $YMnO_3$ films seems to be between 225 and 300 °C, but in practice, the films deposited at 225 °C were of lower quality in terms of thickness variations. For $TbMnO_3$, the observed temperature range of ALD-type growth is slightly narrower ranging from 275 to 300 °C.

None of the rare-earth manganites had crystallized during the deposition; thus, a postdeposition heat treatment was performed for all the cation-stoichiometric samples. The size of the rare-earth element was found to have little effect on the temperature at which the films were crystallized. For instance, the film thickness has a more significant effect on the crystallization temperature. According to calculations on film/substrate mismatch of $RMnO_3$ and the perovskite substrates $LaAlO_3$ and $SrTiO_3$, the low mismatch with lanthanum aluminate should be the best promoter for the formation of metastable *o*-$RMnO_3$ perovskites. The most successful results on stabilization of the *o*-$RMnO_3$ perovskites with the small R constituents were indeed obtained when depositing the film on $LaAlO_3$ (Table 2). In fact, single-phase $RMnO_3$ perovskite samples were obtained on $LaAlO_3$ for all the Rs investigated in this study. As seen in Figure 3, orthorhombic $YbMnO_3$ contained minor amounts of hexagonal impurity when deposited on $SrTiO_3$, whereas the film deposited on $LaAlO_3$ was of single-phase *o*-$YbMnO_3$. Hexagonal $YbMnO_3$ was obtained on silicon at 900 °C but was found to decompose at 1000 °C forming binary oxide impurities. Similar behavior was observed for *h*-$LuMnO_3$ as well, even though higher temperatures are known to favor the formation of the hexagonal structure in bulk samples.[28−30] Not surprisingly, the crystal structures for the larger rare earths were less affected by the substrate crystals used and, as presented in Figure 4, single-phase orthorhombic $SmMnO_3$ was obtained on all the attempted substrates. An exception to the rule was given by $TbMnO_3$ deposited on $SrTiO_3$ which resulted in the formation of either $Tb_2Mn_2O_7$ or $TbMn_2O_5$. Moreover, the distinction between orthorhombic and rhombohedral perovskite structures of $LaMnO_3$ was rather challenging considering the methods available, but the preparation conditions, including the presence of ozone, are likely to favor the formation of rhombohedral, cation-deficient $La_{1-\varepsilon}Mn_{1-\varepsilon}O_3$. In general, the crystal structure of $RMnO_3$ could be well controlled by simply choosing an appropriate substrate crystal, and the minor amounts of impurities observed in the samples consisted of either binary oxide impurities or hexagonal phase of the $RMnO_3$ in question.

The temperature dependencies of magnetization for the $SmMnO_3$ thin-film samples deposited on silicon, $LaAlO_3$, and $SrTiO_3$ are shown in Figure 5. The observed Néel temperature is ∼60 K in all the cases, regardless of the substrate material and well in agreement with results on powder samples.[31] Most of the measurements were, however, performed on $RMnO_3$ samples deposited on $LaAlO_3$ as these samples contained the least amount of impurities. The poor crystallinity of hexagonal phases caused some difficulties in the magnetization measurements, and collecting good-quality data proved to be challenging despite several attempts. Moreover, although qualitative interpretations based on magnetization measurements of thin-film samples can be done reliably, care should be taken while making any conclusions based on absolute values obtained from the data as several factors, such as the degree of crystallinity of the film, can affect the magnitude of the magnetic susceptibility. For *o*-$RMnO_3$, the temperature dependence of magnetization revealed the expected antiferromagnetic properties as seen in Figure 6 where *o*-$YMnO_3$ and *o*-$TbMnO_3$ were chosen as representative examples. The Néel temperature for both *o*-$YMnO_3$ deposited on $LaAlO_3$ and *o*-$TbMnO_3$ deposited on silicon is 40 K which is in good accordance with studies performed on powder samples.[32,33] The magnetization measurements showed ferromagnetic interactions in the $La_{1-\varepsilon}Mn_{1-\varepsilon}O_3$ sample below the Curie temperature (T_C) of 175 K giving reason to believe that the sample preparation through ALD and subsequent annealing at 1000 °C in N_2 flow does not result in a stoichiometric sample. In order to confirm that the oxygen nonstoichiometry of $LaMnO_3$ thin films can be easily affected through alterations in the annealing conditions, the lattice parameters of $LaMnO_3$ samples (deposited on silicon) annealed at 800 °C in nitrogen and oxygen flow were determined. A slight deviation was indeed observed in the lattice parameters of rhombohedral-type structure[34,35] with *a* and α increasing from 5.434(8) Å and 60.519(6)° (O_2 flow) to 5.450(1) Å and 60.610(2)° (N_2 flow) with decreasing partial pressure of oxygen, thus indicating a decrease in oxygen content/an increase in the concentration of cation vacancies in the structure.

dx.doi.org/10.1021/cm103480d |*Chem. Mater.* 2011, 23, 1835–1840

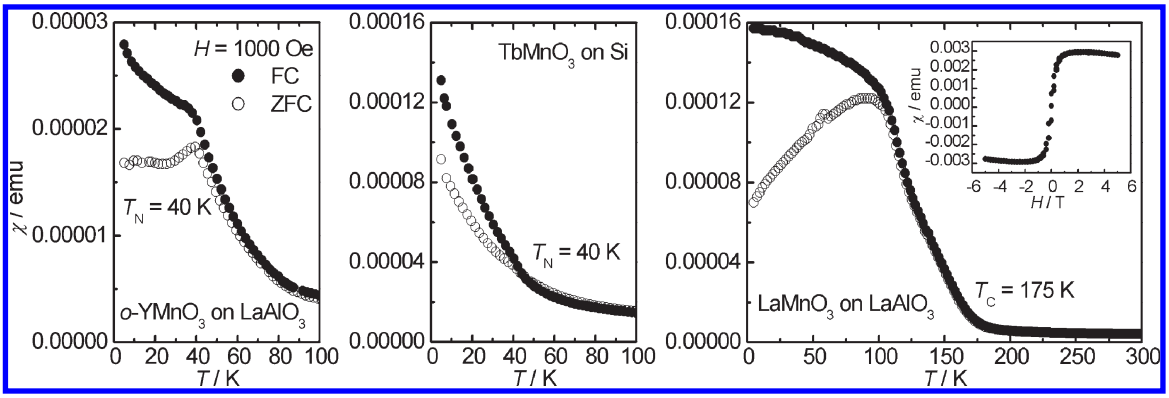

Figure 6. Temperature dependence of magnetic susceptibility (χ) in ZFC and FC modes under an external field of 1000 Oe for *o*-$YMnO_3$ on $LaAlO_3$, $TbMnO_3$ on silicon, and $La_{1-x}Mn_{1-x}O_3$ on $LaAlO_3$. Inset: field dependence of magnetic susceptibility (measured at 5 K) of a $La_{1-x}Mn_{1-x}O_3$ film deposited on $LaAlO_3$.

4. CONCLUSIONS

An extensive series of high-quality thin-film samples of the $RMnO_3$ perovskite family has been fabricated employing the ALD technique and a subsequent heat treatment. The formation of the metastable orthorhombic $RMnO_3$ perovskites of the small rare earths was successfully promoted even for the smallest R constituent of Lu by depositions on coherent perovskite substrates with low lattice mismatch with the targeted structure. High-quality samples were obtained especially on lanthanum aluminate substrates on which the entire series of $RMnO_3$ perovskites from R = La to Lu could be obtained. Due to close to linear dependency between the actual cation ratio and the cation pulsing ratio, the fabrication of essentially cation-stoichiometric samples was rather an easy task. The results of magnetization measurements were in good accordance with earlier studies on powder samples. The ferromagnetic interactions in the $La_{1-\varepsilon}Mn_{1-\varepsilon}O_3$ sample revealed the presence of cation vacancies in the structure. For R = Y, Yb, and Lu, deposition of $RMnO_3$ thin films with the hexagonal structure (after postdeposition annealing) was successfully realized when Si as a substrate material was used.

AUTHOR INFORMATION

Corresponding Author

*Phone: +358-9-470-22600. Fax: +358-9-462 373. E-mail: maarit.karppinen@tkk.fi.

ACKNOWLEDGMENT

This work was supported by Academy of Finland (Nos. 116254 and 126528) and Finnish Foundation for Technology Promotion.

REFERENCES

(1) Yakel, H. L., Jr. *Acta Crystallogr.* **1955**, *8*, 394.
(2) Yakel, H. L., Jr.; Koehler, W. C.; Bertaut, E. F.; Forrat, F. *Acta Crystallogr.* **1963**, *16*, 957.
(3) Huang, Z. J.; Cao, Y.; Sun, Y. Y.; Xue, Y. Y.; Chu, C. W. *Phys. Rev. B* **1997**, *56*, 2623.
(4) Fiebig, M.; Lottermosser, Th.; Fröhlich, D.; Goltsev, A. V.; Pisarev, R. V. *Nature* **2002**, *419*, 818.
(5) Kimura, T.; Goto, T.; Shintani, H.; Ishizaka, K.; Arima, T.; Tokura, Y. *Nature* **2003**, *426*, 55.
(6) Yen, F.; dela Cruz, C.; Lorenz, B.; Galstyan, E.; Sun, Y. Y.; Gospodinov, M.; Chu, C. W. *J. Mater. Res.* **2007**, *22*, 2163.
(7) Bertaut, E. F.; Forrat, E. F.; Fang, P. H. *C. R. Acad. Sci. Paris* **1963**, *265*, 1958.
(8) Hwang, H. Y.; Cheong, S.-W.; Radaelli, P. G.; Marezio, M.; Batlogg, B. *Phys. Rev. Lett.* **1995**, *75*, 914.
(9) Von Helmolt, R.; Wecker, J.; Holzapfel, B.; Schultz, L.; Samwer, K. *Phys. Rev. Lett.* **1993**, *71*, 2331.
(10) Voorhoeve, R. J. H.; Remeika, J. P.; Freeland, P. E.; Matthias, B. T. *Science* **1972**, *177*, 353.
(11) Levasseur, B.; Kaliaguine, S. *J. Solid State Chem.* **2008**, *181*, 2953.
(12) Putkonen, M.; Sajavaara, T.; Niinistö, L.; Keinonen, J. *Anal. Bioanal. Chem.* **2005**, *382*, 1791.
(13) Nilsen, O.; Rauwel, E.; Fjellvåg, H.; Kjekshus, A. *J. Mater. Chem.* **2007**, *17*, 1466.
(14) Nilsen, O.; Peussa, M.; Fjellvåg, H.; Niinistö, L.; Kjekshus, A. *J. Mater. Chem.* **1999**, *9*, 1781.
(15) Uusi-Esko, K.; Malm, J.; Karppinen, M. *Chem. Mater.* **2009**, *21*, 5691.
(16) Eisentraut, K. J.; Sievers, R. E. *J. Am. Chem. Soc.* **1956**, *87*, 5254.
(17) Hammond, G. S.; Nonhebel, D. C.; Wu, C.-H. S. *Inorg. Chem.* **1963**, *2*, 73.
(18) Putkonen, M.; Sajavaara, T.; Johansson, L.-S.; Niinistö, L. *Chem. Vap. Deposition* **2001**, *7*, 44.
(19) Nilsen, O.; Rauwel, E.; Fjellvåg, H.; Kjekshus, A. *J. Mater. Chem.* **2007**, *17*, 1466.
(20) *UniQuant Version 2 User Manual*; Omega Data Systems: Neptunus 2, NL-5505 Veldhoven, The Netherlands, 1994.
(21) Rodriguez-Carvajal, J.; Hennion, M.; Moussa, F.; Moudden, A. H.; Pinsard, L.; Revcolevschi, A. *Phys. Rev. B* **1998**, *57*, R3189.
(22) Nilsen, O.; Fjellvåg, H.; Kjekshus, A. *Thin Solid Films* **2003**, *444*, 44.
(23) Päiväsaari, J.; Putkonen, M.; Niinistö, L. *Thin Solid Films* **2005**, *472*, 275.
(24) Nieminen, M.; Putkonen, M.; Niinistö, L. *Appl. Surf. Sci.* **2001**, *174*, 155.
(25) Binnemans, K. In *Handbook on the Physics and Chemistry of Rare Earths*; Gschneider, K. A., Jr., Bünzli, J.-C. G., Percharsky, V. K., Eds.; Elsevier: Amsterdam, 2005; Vol. 35, pp 107−272.
(26) Martynenko, L. I.; Kuz'mina, N. P.; Grigor'ev, A. N. *Russ. J. Inorg. Chem.* **1998**, *43*, 1038.
(27) De Villiers, J. P. R.; Boyens, J. C. A. *Acta Cryst. B* **1972**, *28*, 2335.
(28) Brinks, H. W.; Fjellvåg, H.; Kjekshus, A. *J. Solid State Chem.* **1997**, *129*, 334.
(29) Alonso, J. A.; Martínez-Lope, M. J.; Casais, M. T. *Inorg. Chem.* **2000**, *39*, 917.
(30) Uusi-Esko, K.; Malm, J.; Imamura, N.; Yamauchi, H.; Karppinen, M. *Mater. Chem. Phys.* **2008**, *112*, 1029.

(31) Zhou, J.-S.; Goodenough, J. B. *Phys. Rev. B* **2003**, *68*, 054403.
(32) Katsufuji, T.; Masaki, M.; Machida, A.; Moritomo, M.; Kato, K.; Nishibori, E.; Takata, M.; Sakata, M.; Ohoyama, K.; Kitazawa, K.; Takagi, H. *Phys. Rev. B* **2002**, *66*, 134434.
(33) Argyriou, D. N.; Aliouane, N.; Strempfer, J.; Zegkinoglou, I.; Bohnenbuck, B.; Habicht, K.; v. Zimmermann, M. *Phys. Rev. B* **2007**, *75*, 020101.
(34) Töpfer, J.; Goodenough, J. B. *J. Solid State Chem.* **1997**, *130*, 117.
(35) Alonso, J. A.; Martínez-Lope, M. J.; Casais, M. T.; MacManus-Driscoll, J. L.; de Silva, P. S. I. P. N.; Cohen, L. F.; Fernández-Díaz, M. T. *J. Mater. Chem.* **1997**, *7*, 2139.